Hindawi
Advances in Materials Science and Engineering
Volume 2017, Article ID 5821835, 9 pages
https://doi.org/10.1155/2017/5821835

Research Article

Comparison of Damage Detection Methods Depending on FRFs within Specified Frequency Ranges

Yong-Su Kim[1] and Hee-Chang Eun[2]

[1]*Department of Architectural Engineering, Chung-Ang University, Seoul, Republic of Korea*
[2]*Department of Architectural Engineering, Kangwon National University, Chuncheon, Republic of Korea*

Correspondence should be addressed to Hee-Chang Eun; heechang@kangwon.ac.kr

Received 8 April 2017; Accepted 20 July 2017; Published 29 August 2017

Academic Editor: Xiao-Jian Gao

Structural damage can be detected using frequency response function (FRF) measured by an impact and the corresponding responses. The change in the mechanical properties of dynamic system for damage detection can seldom be estimated using FRF data extracted from a very limited frequency range. Proper orthogonal modes (POMs) from the FRFs extracted in given frequency ranges and their modified forms can be utilized as damage indices to detect damage. The POM-based damage detection methods must be sensitive to the selected FRFs. This work compares the effectiveness of the damage detection approaches taking the POMs estimated by the FRFs within five different frequency ranges including resonance frequency and antiresonance frequency. It is shown from a numerical example that the POMs extracted from the FRFs within antiresonance frequency ranges provide more explicit information on the damage locations than the ones within resonance frequency ranges.

1. Introduction

Structural damage is detected based on the variation in dynamic responses due to the local change of physical properties at damage region. There have been many attempts to provide the accurate damage detection methods related to structural health monitoring. Many indices like mode shapes, mode shape curvature, frequency response function (FRF) curvature, modal strain energy, and so forth to evaluate the structural performance have been utilized [1, 2].

One of the measurement data types is FRF data set. The FRF can be estimated by impact hammer test and the energy is propagated from the impact point. The FRF data measured from experimental work are utilized to estimate the characteristics of dynamic system. It indicates that the measured FRF data set can be used as an index to detect damage. Phani and Woodhouse [3] proposed the FRF curvature method based on only the measured data without the need for any modal identification. Lee and Kim [4] proposed a structural damage detection method to determine both location and magnitude of damage from perturbation equations of FRF data. Fritzen [5] evaluated a FRF-based model updating algorithm using experimentally collected data and presented a protocol for measurement selection and a regularization technique. Rahmatalla et al. [6] presented a feasible method for structural vibration-based health monitoring to reduce the dimension of the initial FRF data and to employ artificial neural network. Sampaio et al. [7] provided a structural damage identification technique using changes of the FRF to be related to the changes of the stiffness and mass through damage sensitivity equations. Wang et al. [8] developed a methodology by coupled response monitoring through the emergence of peaks on a FRF plot to determine the damage existence. Garcia-Palencia et al. [9] exhibited that the curvatures of FRF at frequencies other than natural frequencies can be used for identifying both the existence of damage and the location of damage. Bandara et al. [10] presented a damage identification method using the changes in the distribution of the compliance of the structure due to damage. Bandara et al. [11] investigated the advantages and limitations to use vibration-based damage detection methods from the measurements of mode shapes

and FRFs. Nozarian and Esfandiari [12] identified parameter matrices using FRF data measured at specific positions and constraints and provided a damage detection method from their variations.

Proper orthogonal decomposition (POD) analysis captures most of the kinetic energy in the least number of modes possible. Its application is similar to that of Fourier analysis, except that it normally requires far less modes to represent the system within a desired level. POMs extracted from the FRF data in a prescribed frequency range are utilized as an index to recognize the existence of damage. The POD method has been widely applied in various fields of engineering and science. Ramanamurthy et al. [13] related the POM to normal modes of vibration in systems for lightly modally damped systems. They exhibited that the POMs represent the principal axes of inertia formed by the distribution of data on the modal coordinate curve. Using statistical process control technique, Mondal et al. [14] investigated the applications of principal component analysis for damage diagnosis. Choi et al. [15] provided a damage detection algorithm based on the POD technique to filter out the influence of operational/environmental variation in the dynamic response. De Medeiros et al. [16] applied a POD statistical method to the field of damage detection for continuous static monitoring systems. Feeny and Kappagantu [17] presented a damage detection method based on fuzzy c-means clustering algorithm and measured FRF data reduced by principal component analysis. De Boe and Golinval [18] developed a POMs-based damage identification approach using acceleration dynamic responses of shear-type buildings. Shane and Jha [19] presented a neural networks-based damage detection method using FRF data. The method reduces the dimension of the initial FRF data and employs an artificial neural network for the actual damage.

The parameter matrices as well as damage region of dynamic systems can be predicted using FRF data sets within a specific frequency range rather than at a specific frequency. The FRF data sets are transformed to the POM to represent the principal axes of inertia formed by the distribution of data on the modal coordinate curve. The POM can be changed depending on the FRF data sets extracted from full sets of FRFs. Beginning with the FRFs measured from the dynamic finite element model, this work investigates the sensitivity of the damage detection method using the POMs to be estimated from the FRFs corresponding to five different frequency ranges including resonance frequency and antiresonance frequency. A numerical example compares the sensitivity of the damage detection method depending on the extracted FRFs.

2. FRF and POM

The dynamic behavior of a structure, which is assumed to be linear and approximately discretized for n DOFs, can be described by the equations of motion:

$$\mathbf{M}\ddot{\mathbf{u}} + \mathbf{C}\dot{\mathbf{u}} + \mathbf{K}\mathbf{u} = \mathbf{F}(t), \tag{1}$$

where $\mathbf{M}$, $\mathbf{K}$, and $\mathbf{C}$ denote the $n \times n$ analytical mass, stiffness, and damping matrices, respectively, $\mathbf{u} = [u_1 \ u_2 \ \cdots \ u_n]^T$, and $\mathbf{F}(t)$ is the $n \times 1$ load excitation vector.

Frequency response function $\mathbf{H}(\Omega)$ is defined as the ratio of the complex spectrum of the response to the complex spectrum of the excitation:

$$\mathbf{H}(\Omega) = \frac{\mathbf{U}(\Omega)}{\mathbf{F}(\Omega)}, \tag{2}$$

where $\mathbf{U}(\Omega)$ and $\mathbf{F}(\Omega)$ denote the complex spectrum of the response and the complex spectrum of the excitation, respectively. The magnitude of the FRF $|\mathbf{H}(\Omega)|$ denotes the ratio of $|\mathbf{U}(\Omega)|/|\mathbf{F}(\Omega)|$.

For the case of a displacement response at station p and a disturbing force at station q, the numerical frequency response can be constructed as

$$H_{pq}(\Omega) = \sum_{i=1}^{n} \frac{\phi_{ip}\phi_{iq}}{\omega_i^2 - \Omega^2 + 2j\xi_i\omega_i\Omega}, \tag{3}$$

where ϕ_{ip} denotes the pth element of the vector ϕ_i and ω_i and ξ_i denote the circular natural frequency and the damping ratio, respectively, for the ith mode, $j = \sqrt{-1}$.

The FRF data, $\widehat{H}_{pq}$, contaminated by external noise rarely provide the accurate information on the dynamic system. In this study, they can be described by adding a series of random numbers to the calculated FRF response data expressed by

$$\widehat{H}_{pq} = H_{pq}\left(1 + \alpha\sigma_{pq}\right), \tag{4}$$

where α denotes the relative magnitude of the error, and σ_{pq} is a random number variant in the range $[-1, 1]$.

The measured FRFs can be reduced by the POD and are transformed to the POD to extract extremal data set. The POD technique is effective method because basis elements are formed in an optimal way. The POD basis collects snapshots. The FRFs of a system are generated by forcing the system. $H_{pq}(\Omega)$ expresses an FRF on a finite number of points in space and a finite frequency interval $\Omega_{\min} \le \Omega \le \Omega_{\max}$. The FRFs at n dofs are sampled m frequencies and the data are arranged in a snapshot matrix $\widehat{\mathbf{H}}$:

$$\widehat{\mathbf{H}} = \begin{bmatrix} \widehat{H}_{1q}(\Omega_1) & \widehat{H}_{1q}(\Omega_2) & \cdots & \widehat{H}_{1q}(\Omega_m) \\ \widehat{H}_{2q}(\Omega_1) & \widehat{H}_{2q}(\Omega_2) & \cdots & \widehat{H}_{2q}(\Omega_m) \\ \vdots & \vdots & \ddots & \vdots \\ \widehat{H}_{nq}(\Omega_1) & \widehat{H}_{nq}(\Omega_2) & \cdots & \widehat{H}_{nq}(\Omega_m) \end{bmatrix}_{n\times m}. \tag{5}$$

Let the $m \times m$ autocovariance matrix $\mathbf{C}$ be defined as

$$\mathbf{C} = \mathbf{H}_{mea}^T\mathbf{H}_{mea}, \tag{6}$$

where m is the number of the FRF data sets extracted. Matrix $\mathbf{C}$ is a Hermitian positive semidefinite matrix to possess a complete set of orthogonal eigenvectors with corresponding nonnegative real eigenvalues. Solving the eigenvalue problem of (6) at the core of the POD method, (6) satisfies

$$\mathbf{C}\boldsymbol{\varphi}_k = \lambda_k\boldsymbol{\varphi}_k, \quad k = 1, \ldots, m, \tag{7}$$

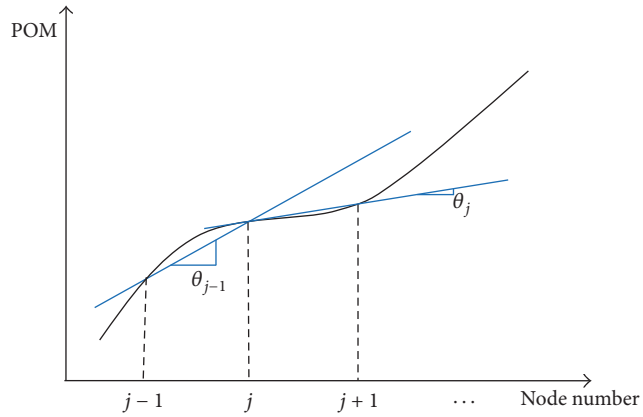

Figure 1: Slope of POM.

where the eigenvalues reflect the energies in different POMs and are arranged in descending order as follows:

$$\lambda_1 \geq \lambda_2 \geq \cdots \geq \lambda_m \geq 0, \tag{8}$$

where the eigenvalues λ_k are the POVs, and the corresponding eigenvector $\boldsymbol{\varphi}_k$ of the extreme value problem is associated with a POV λ_k. The greatest POV is the optimal vector to characterize the snapshots.

The POMs may be used as a basis for the decomposition of $\mathbf{H}_{mea}$. The POM associated with the greatest POV is the optimal vector. If the eigenvalues are normalized to unit magnitude, then they represent the relative energy captured by the corresponding POM. The eigenvalue reflects the relative kinetic energy associated with the corresponding mode. The energy is defined as the sum of the POVs. The POMs are written as

$$\boldsymbol{\psi}^k = \frac{\widehat{\mathbf{H}}\boldsymbol{\varphi}_k}{\left\|\widehat{\mathbf{H}}\boldsymbol{\varphi}_k\right\|}, \quad k = 1, \ldots, m, \tag{9}$$

where $\widehat{\mathbf{H}}$ denotes the $m \times m$ FRF matrix in (5) and $\boldsymbol{\varphi}_k$ represents the $m \times 1$ eigenvector corresponding to the eigenvalue λ_k. The POMs $\boldsymbol{\psi}$ are arranged as follows:

$$\boldsymbol{\psi} = \left[\boldsymbol{\psi}^1 \;\; \boldsymbol{\psi}^2 \;\; \cdots \;\; \boldsymbol{\psi}^m\right]. \tag{10}$$

The slope of the POM data corresponding to two adjacent nodes from Figure 1 can be defined as

$$\theta_j = \frac{\boldsymbol{\psi}^1_{j+1} - \boldsymbol{\psi}^1_j}{h}, \quad j = 1, 2, \ldots, n-1, \tag{11}$$

where h is the distance between two adjacent nodes. The sum of the squared slope of the POM at two adjacent nodes is defined as

$$\eta_j = \theta_j^2 + \theta_{j+1}^2, \quad j = 1, 2, \ldots, n-2. \tag{12}$$

Damage introduced into the flexural beam to be modeled as finite elements also leads to local changes in the shape of POM curvature obtained by POMs. The curvature at each location j on the structure, $\boldsymbol{\psi}''_j$, is numerically obtained by a central difference approximation:

$$\boldsymbol{\psi}''_j = \frac{\boldsymbol{\psi}_{j-1} - 2\boldsymbol{\psi}_j + \boldsymbol{\psi}_{j+1}}{h^2}, \quad j = 2, 3, \ldots, n-1, \tag{13}$$

where $\boldsymbol{\psi}''_j$ is the second derivatives at the jth node and h is the distance between two successive nodes. The damage is evaluated by the POM curvature extracted from the measured FRFs without the baseline data.

3. Numerical Experiment

A numerical experiment was performed in detecting the damage in a finite element model of a three-span continuous beam shown in Figure 2 to examine the validity of the proposed method depending on the selected FRF data sets. The nodal points and the elements are numbered as shown in the figure. The continuous beam with a length of 9 m is modeled using 100 beam elements. The beam has an elastic modulus of 2.0×10^5 MPa and a unit mass of 7,860 kg/m^3. The beam's gross cross section is 500 mm × 200 mm, and its damage section is established as 90% of the moment of inertia of the undamaged beam. The damping matrix is assumed as a Rayleigh damping to be expressed by the stiffness matrix and a proportionality constant of 0.0001. This application considers the damage detection of a beam with multiple damage at elements ⑤⑤ and ⑧⑤. The FRF data are numerically simulated by the responses at all nodes due to the impact at node 18. The measurement data in (4) include 1% external noise.

The damage leads to the local stiffness deterioration and the variation of the natural frequencies. Its existence can be recognized through the comparison with the natural frequencies at the undamaged state. The first three natural frequencies of the damaged dynamic system exist at 24.67 Hz, 40.89 Hz, and 69.69 Hz, respectively. Figure 3(a) represents the mode shapes corresponding to the first, second, and third natural frequencies, respectively. The damage can be detected by the comparison of the mode shapes at both states. However, it is not easy to collect the accurate mode shapes

Table 1: Frequency ranges of the extracted FRFs.

Location	(A)	(B)	(C)	(D)	(E)
Selected frequencies	10 Hz ± 0.1 Hz	24.67 Hz ± 0.1 Hz	34.25 Hz ± 0.1 Hz	40.89 Hz ± 0.1 Hz	50.93 Hz ± 0.1 Hz
	Less than first resonance	Resonance	Antiresonance	Resonance	Antiresonance

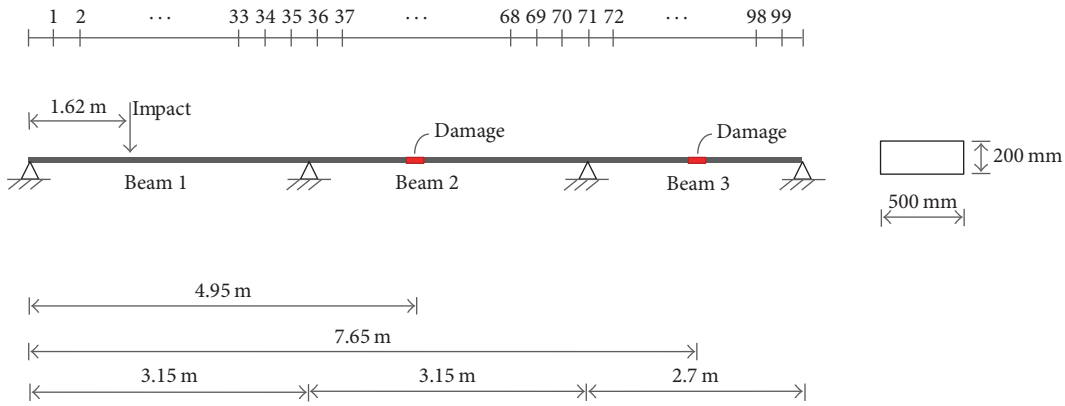

Figure 2: A three-span continuous beam structure model.

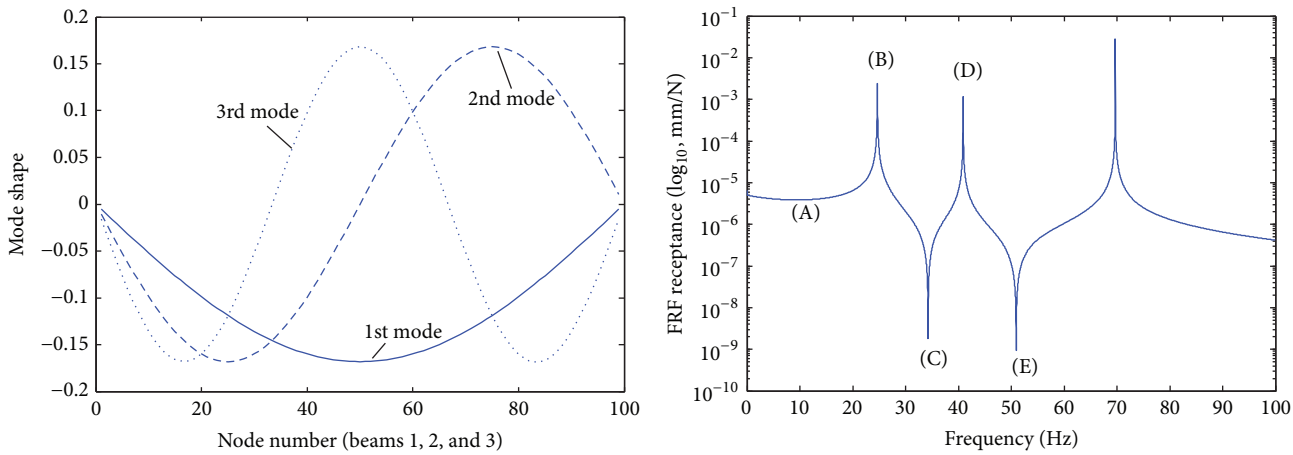

Figure 3: Dynamic characteristics of the system: (a) mode shapes and (b) FRF curve.

corresponding to the resonance frequencies due to external noise. Thus this work utilizes a set of FRFs and they are transformed to the POM to take extremal data set. Figure 3(b) displays the FRF receptance curve of the responses at all nodes due to a single impact at node 18. It is shown that the first three resonance frequencies coincide with the natural frequencies. The resonance frequencies correspond to the peaks in the plots and the antiresonance frequencies correspond to the valleys.

This numerical study investigates the sensitivity of the damage detection depending on the FRFs extracted in the neighborhood of two resonance frequency ranges at points (B) and (D) in Figure 3(b), two antiresonance frequency ranges at points (C) and (E), and point (A) less than the first resonance frequency in Figure 3(b). The FRFs were calculated at the intervals of 0.02 Hz for this numerical experiment. Eleven FRF data sets simulated in the frequency range of ±0.1 Hz from the resonance and antiresonance frequencies are extracted to establish the POMs as shown in Table 1.

Figure 4 represents the normalized POM curve of beams 1, 2, and 3 corresponding to the first POV depending on the noise-free FRFs in the selected five frequency ranges shown in Figure 3(b). Figure 4(a) displays the POM curves of beam 1 depending on the FRFs to be chosen. It is observed that the POM plots corresponding to the first resonance frequency (B) and its neighboring frequency (A), and the second frequency (D) and its neighboring frequency (E) are very similar except the curve (C) corresponding to the antiresonance frequency. The valley of the curve corresponding to (C) corresponds to the impact location. Figure 4(b) represents the POM curves

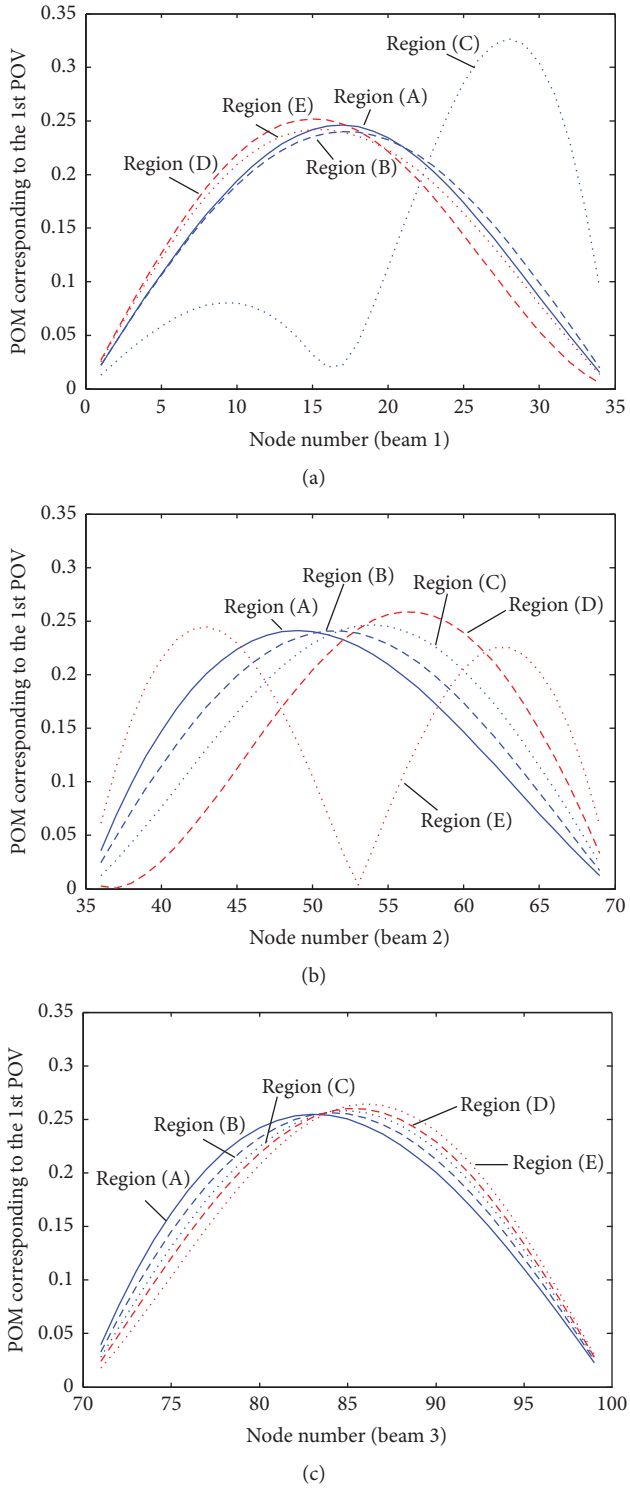

FIGURE 4: POM curves using noise-free FRFs within the five different frequency ranges: (a) beam 1, (b) beam 2, and (c) beam 3.

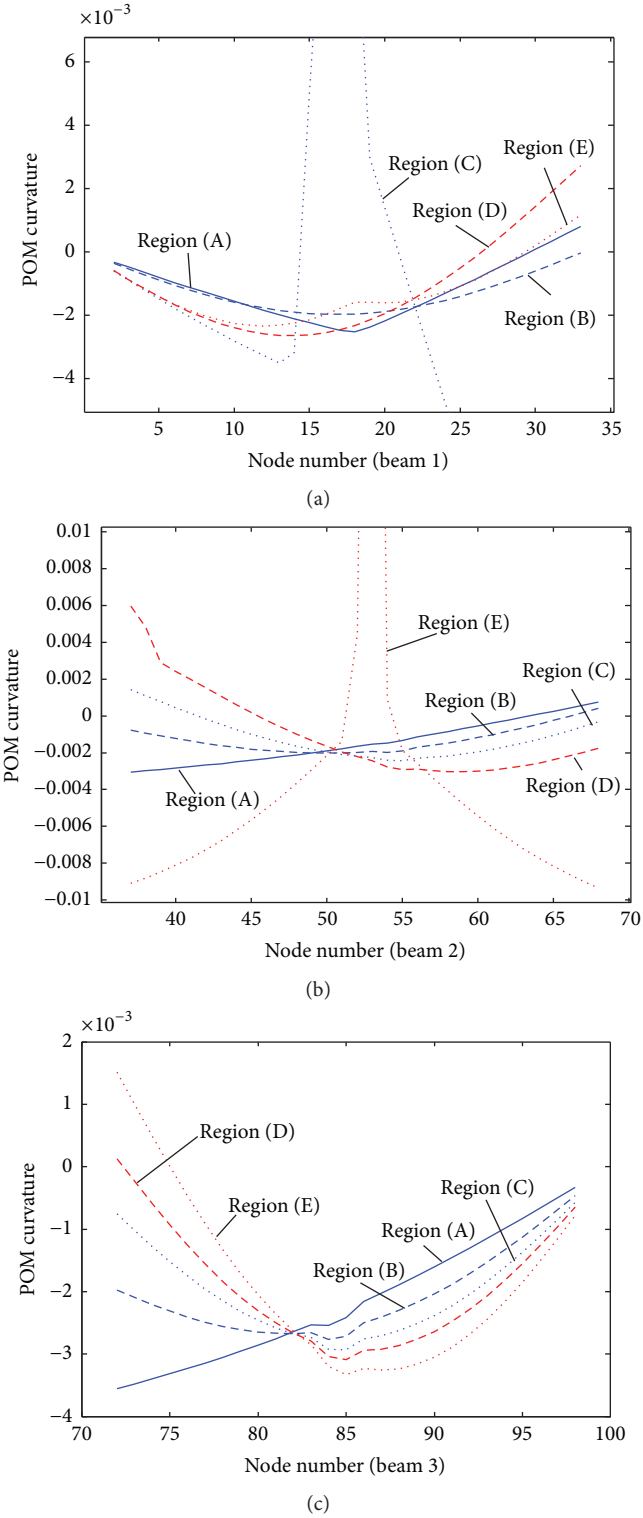

FIGURE 5: POM curvature curves using noise-free FRFs: (a) beam 1, (b) beam 2, and (c) beam 3.

of beam 2. It is shown that the peak of the curves moves little by little to the right with the increase of the frequency region to extract the FRF data except the POM curve corresponding to region (E). Figure 4(c) exhibits the POM curves of beam 3. The peak of the curves moves little by little to the right with the increase of the frequency region to extract the FRF data. It is found that the plots in Figure 4 do not provide the information on the damage in the beam.

Figure 5 exhibits the POM curvature curves approximated numerically using the central difference method

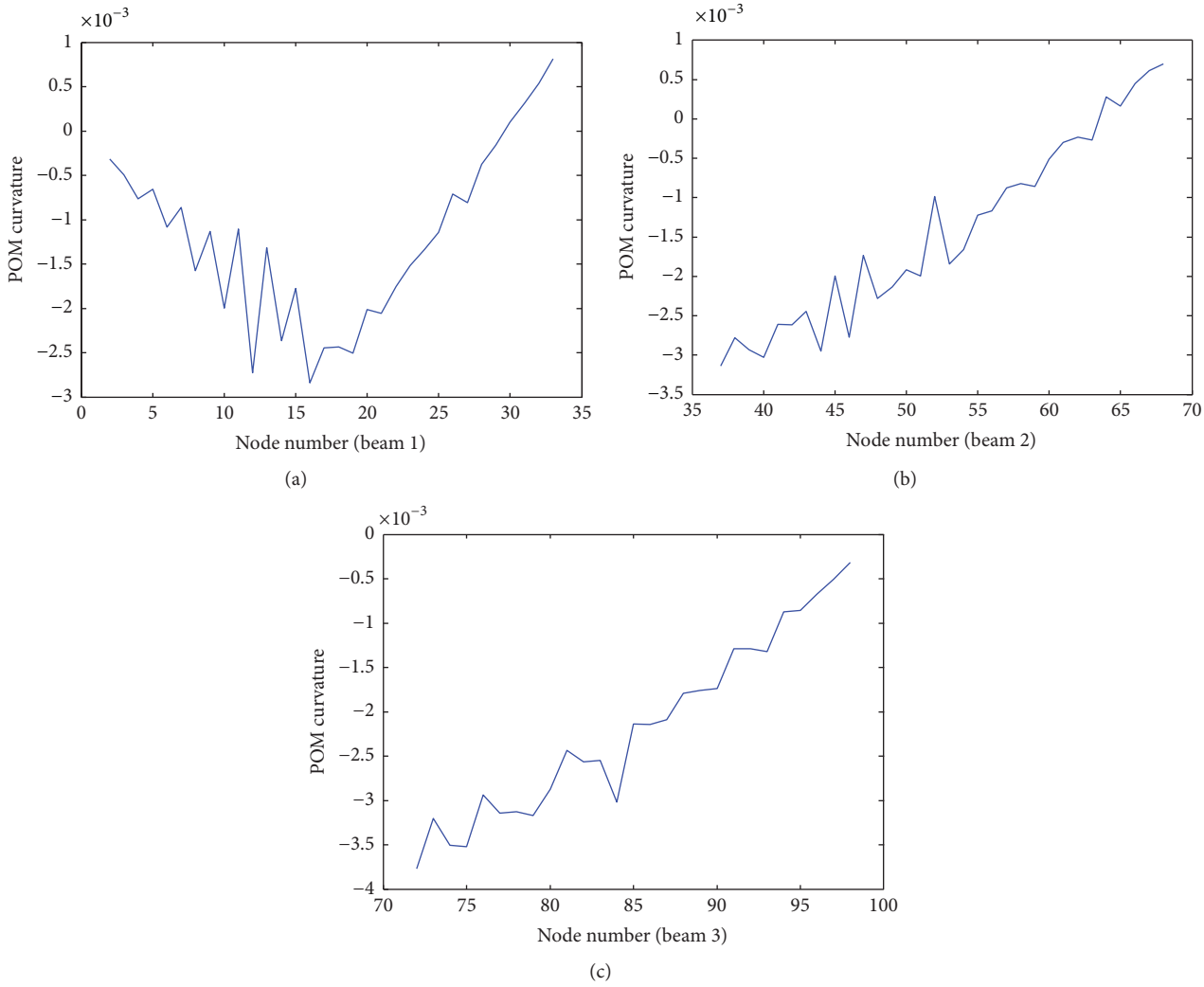

Figure 6: POM curvature curves using FRFs in the region (A) containing 1% external noise: (a) beam 1, (b) beam 2, and (c) beam 3.

of (11). The damage locates at the region to display the abrupt variation of the curvature curve. The impact at node 18 of beam 1 leads to the abrupt change of the POM curvature curve as shown in Figure 5(a). Curve (E) in Figure 4(b) looks like the second mode shape to take the absolute. The abrupt change in the neighborhood of the inflection point is observed. Except those variations, the local change in the neighborhood of elements ⑤⑤ and ⑧⑤ is observed. It is observed that the noise-free POM curvature curves taken from the FRF data of the first four regions shown in Table 1 properly indicate the damage regions.

Figures 6–10 display the POM curvature curves estimated from the FRF data corresponding to the five different frequency regions. The simulated FRF data contain 1% external noise in (4). The plots exhibit the large and small variations of the curvature due to the presence of the external noise so that the damage cannot be detected. The abrupt variation nearby the impact location at node 18 of beam 1 is observed in the plots. Figure 6 represents the plots corresponding to region (B) including the first resonance frequency. It is shown that the POM curve in Figure 6(a) corresponds to first mode shape. The other curves indicate explicitly the damage at the 37th element only. The other damage cannot be recognized because of the noise contained in the measurement data. It is understood that the POM extracted in the first resonance frequency range is sensitive to the external noise.

Figure 7 represents the curves corresponding to region (C) including the second antiresonance frequency. It is found in Figure 7(a) that the POM curve after the impact node 33 does rarely respond and cannot obtain the damage information. The other plots in Figure 7 give the damage information at the 22nd element only and the other damage location cannot be recognized. It is observed that the POM extracted in this region is also sensitive to the external noise.

Figure 8 represents the plots corresponding to region (D) including the second resonance frequency. It is shown that

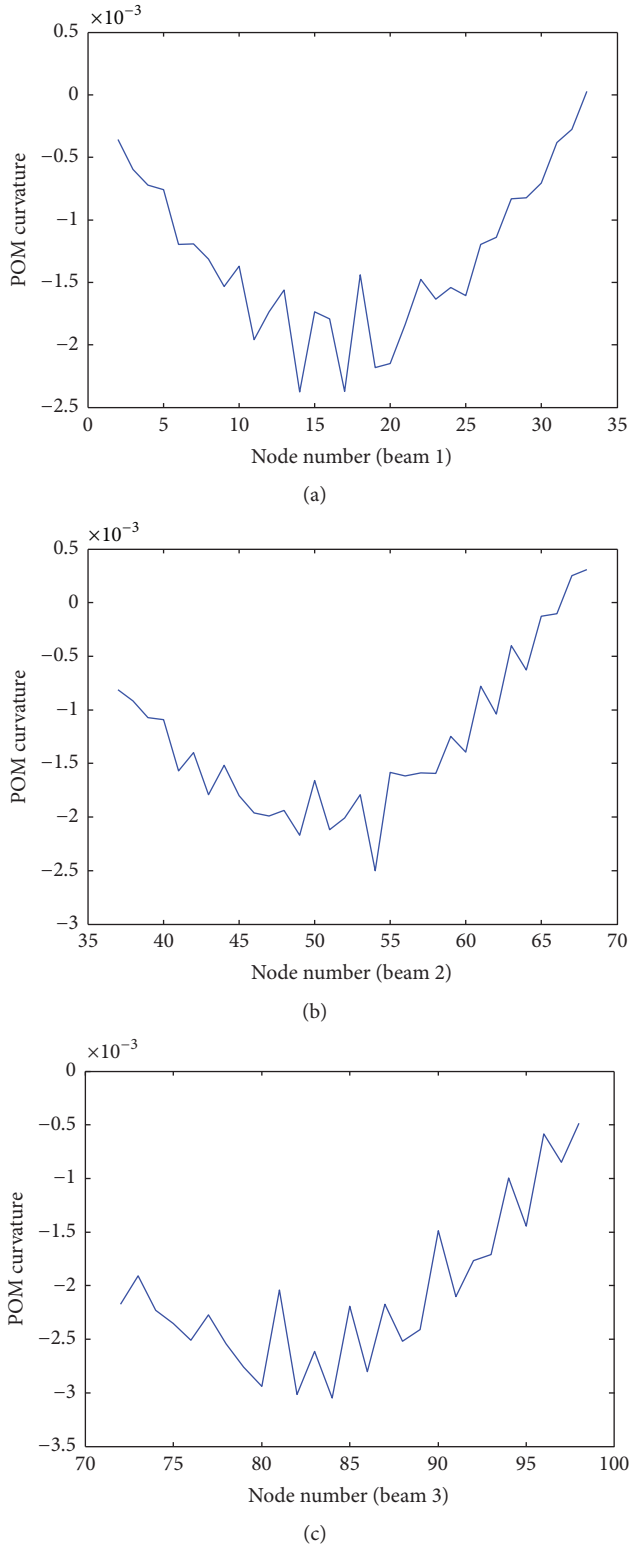

Figure 7: POM curvature curves using FRFs in the region (B) containing 1% external noise: (a) beam 1, (b) beam 2, and (c) beam 3.

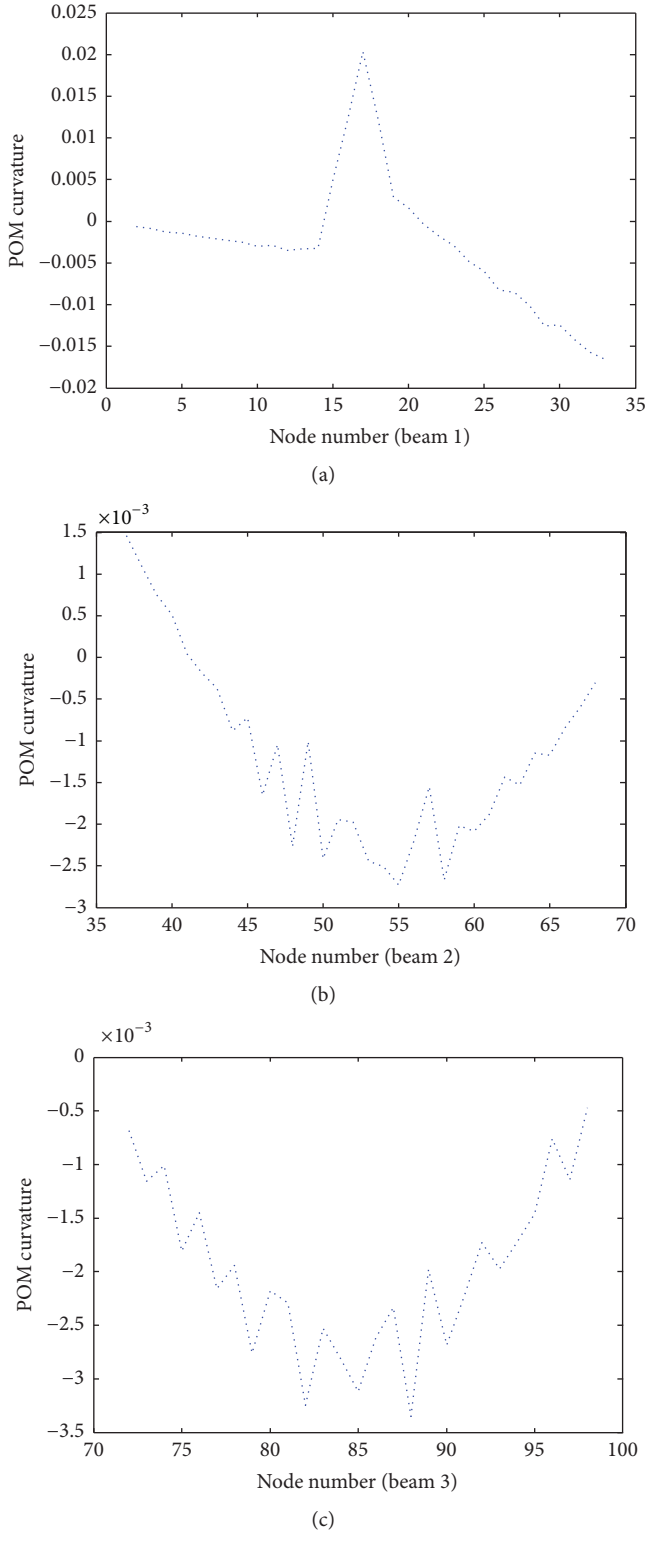

Figure 8: POM curvature curves using FRFs in the region (C) containing 1% external noise: (a) beam 1, (b) beam 2, and (c) beam 3.

the POM curve in Figure 8(a) corresponds to the absolute curve of the second mode shape. It is obtained from Figures 8(b)-8(c) that the damage at the only 22nd element can be explicitly detected and the other damage should be recognized through close examination. The abrupt change of the plots in the center of the span is due to the result that the

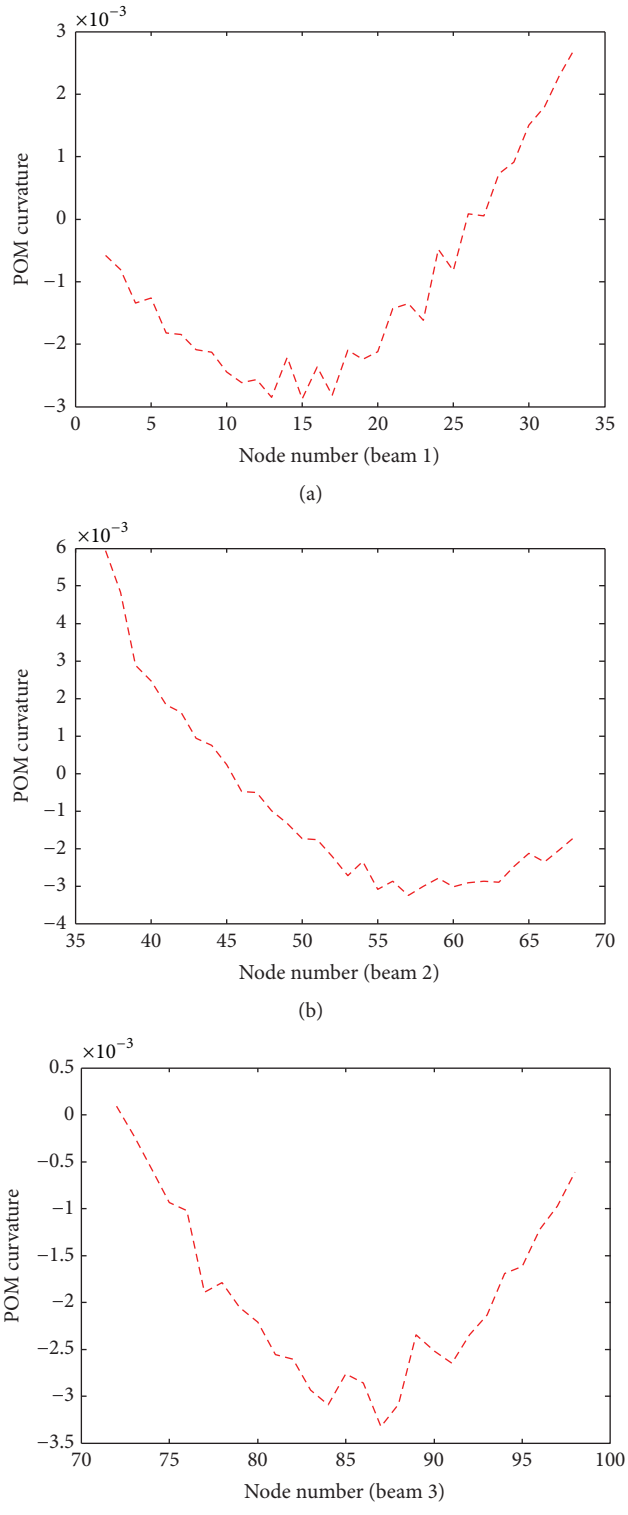

Figure 9: POM curvature curves using FRFs in the region (D) containing 1% external noise: (a) beam 1, (b) beam 2, (c) beam 3.

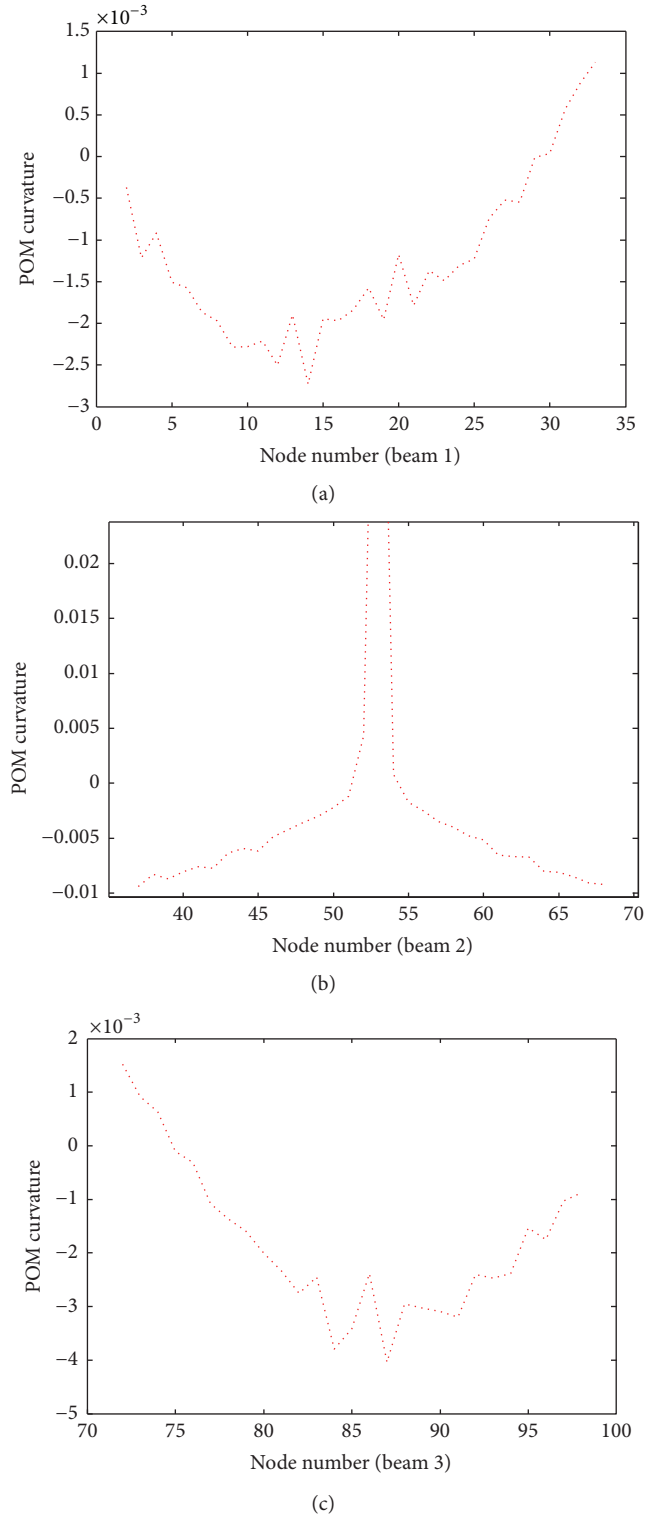

Figure 10: POM curvature curves using FRFs in the region (E) containing 1% external noise: (a) beam 1, (b) beam 2, and (c) beam 3.

POM curve takes the absolute curve as shown in Figure 8(a). It is known that the POM extracted in this region is also sensitive to the external noise.

Figure 9 exhibits the plots corresponding to region (E) including the third antiresonance frequency. It is analyzed that the POM curve in Figure 9(a) cannot obtain any information on the damage location. It is shown that the curves

in Figures 9(b)-9(c) lead to the abrupt variation at the damage locations except impact node 33 and the damage can be explicitly detected. From this numerical experiment, the damage detection method can be explicitly and widely carried out by the three damage indices of the POM corresponding to the first POV to extract the FRFs in the first and third antiresonance frequencies despite the external noise. The POM-based approaches using the FRFs extracted in the other ranges should be sensitive to the external noise and can be utilized by close examination of the POM curve.

4. Conclusions

This work compared the damage detection methods utilizing three different damage indices depending on the extracted FRFs within five different frequency ranges including resonance frequency and antiresonance frequency. It is shown from a numerical example that the damage detection method can be explicitly and widely carried out by the three damage indices of the POM corresponding to the first POV to extract the FRFs in the first and third antiresonance frequencies despite the external noise. The POM-based approaches using the FRFs extracted in the other ranges should be sensitive to the external noise and can be utilized by close examination of the POM curve.

Conflicts of Interest

The authors declare that they have no conflicts of interest.

Acknowledgments

This research is supported by Basic Science Research Program through the National Research Foundation of Korea (NRF) funded by the Ministry of Education (NRF-2016R1D1A1A09918011).

References

[1] S. W. Doebling, C. R. Farrar, M. B. Prime, and D. W. Shevitz, "Damage identification and health monitoring of structural and mechanical systems from changes in their vibration characteristics: a literature review," Tech. Rep. LA-13070-MS, Los Alamos National Laboratory, 1996.

[2] A. K. Pandey, M. Biswas, and M. M. Samman, "Damage detection from changes in curvature mode shapes," *Journal of Sound and Vibration*, vol. 145, no. 2, pp. 321–332, 1991.

[3] A. S. Phani and J. Woodhouse, "Viscous damping identification in linear vibration," *Journal of Sound and Vibration*, vol. 303, no. 3-5, pp. 475–500, 2007.

[4] J.-H. Lee and J. Kim, "Identification of damping matrices from measured frequency response functions," *Journal of Sound and Vibration*, vol. 240, no. 3, pp. 545–565, 2001.

[5] C. P. Fritzen, "Identification of mass and stiffness matrices of mechanical systems," *Journal of Vibration and Acoustics*, vol. 108, pp. 9–16, 1986.

[6] S. Rahmatalla, H.-C. Eun, and E.-T. Lee, "Damage detection from the variation of parameter matrices estimated by incomplete FRF data," *Smart Structures and Systems*, vol. 9, no. 1, pp. 55–70, 2012.

[7] R. P. C. Sampaio, N. M. M. Maia, and J. M. M. Silva, "Damage detection using the frequency-response-function curvature method," *Journal of Sound and Vibration*, vol. 226, no. 5, pp. 1029–1042, 1999.

[8] Z. Wang, R. M. Lin, and M. K. Lim, "Structural damage detection using measured FRF data," *Computer Methods in Applied Mechanics and Engineering*, vol. 147, no. 1-2, pp. 187–197, 1997.

[9] A. Garcia-Palencia, E. Santini-Bell, M. Gul, and N. Catbas, "A FRF-based algorithm for damage detection using experimentally collected data," *Structural Monitoring and Maintenance*, vol. 2, no. 4, pp. 399–418, 2015.

[10] R. P. Bandara, T. H. T. Chan, and D. P. Thambiratnam, "Frequency response function based damage identification using principal component analysis and pattern recognition technique," *Engineering Structures*, vol. 66, pp. 116–128, 2014.

[11] R. P. Bandara, T. H. Chan, and D. P. Thambiratnam, "Structural damage detection method using frequency response functions," *Structural Health Monitoring: An International Journal*, vol. 13, no. 4, pp. 418–429, 2014.

[12] M. M. Nozarian and A. Esfandiari, "Structural damage identification using frequency response function," *Materials Forum*, vol. 33, pp. 443–449, 2009.

[13] E. V. V. Ramanamurthy, K. Changdrasekaran, and N. Gaurav, "Damage identification and location by using the frequency response function in a composite cantilever beam," in *Proceedings of the 3rd World Conference on Applied Sciences, Engineering Technology*, Kathmandu, Nepal, 2014.

[14] S. Mondal, B. Mondal, A. Bhutia, and S. Chakraborty, "Damage detection in beams using frequency response function curvatures near resonating frequencies," *Advances in Structural Engineering: Dynamics, Volume Two*, pp. 1563–1573, 2015.

[15] S. Choi, S. Park, and N. Stubbs, "Nondestructive damage detection in structures using changes in compliance," *International Journal of Solids and Structures*, vol. 42, no. 15, pp. 4494–4513, 2005.

[16] R. De Medeiros, M. Sartorato, F. D. Marques, V. Tita, and D. Vandepitte, "Vibration-based damage identification applied for composite plate: Experimental analysis," in *Proceedings of the 22nd International Congress of Mechanical Engineering*, Brazil, 2013.

[17] B. F. Feeny and R. Kappagantu, "On the physical interpretation of proper orthogonal modes in vibrations," *Journal of Sound and Vibration*, vol. 211, no. 4, pp. 607–616, 1998.

[18] P. De Boe and J. Golinval, "Principal component analysis of a piezosensor array for damage localization," *Structural Health Monitoring: An International Journal*, vol. 2, no. 2, pp. 137–144, 2003.

[19] C. Shane and R. Jha, "Proper orthogonal decomposition based algorithm for detecting damage location and severity in composite beams," *Mechanical Systems and Signal Processing*, vol. 25, no. 3, pp. 1062–1072, 2011.